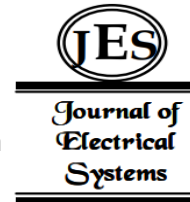


Experimental validation of Extremum Seeking and Sliding Mode-based Control for an autonomous PV System under partial shading conditions



This paper presents an experimental validation of the Extremum Seeking and Sliding mode-based control for an autonomous PV system under uniform and non-uniform irradiance conditions. The modeling of the PV system and the control MPPTs adopted in this study are fully formulated and then implemented via a DSpace 1104 single card. The experimental setup comprises two cases: a healthy state (case 1) and a shaded state with two selected ratios (15% and 5%), which have been used to carry out the results. The obtained results show notable skills of the ESC-based strategy to extract the maximum power under shaded conditions for all the proposed scenarios.

Keywords: DSpace 1104; Extremum Seeking Control (ESC); Maximum Power Point Tracking (MPPT); Shading; PV panel; Sliding Mode Control (SMC).

1. Introduction

Photovoltaic solar energy is one of the most important renewable energy sources. It has attracted much attention in recent research [1-3]. Solar energy is convertible into electrical energy through photovoltaic arrays because of its low maintenance cost, long working life, zero noise, and environment-friendly operation [4]. Despite their advantages, the drawback of solar modules is there is low efficiency (9–17%). Furthermore, it depends on the weather conditions [5]. The I-V as well as the P-V characteristic curves of the solar cell are nonlinear and strongly affected by a number of factors such as solar irradiation, ambient temperature, and applied load [6]. Generally, there is only one particular point on the P-V characteristic curve where the module operates at its maximum efficiency and the maximum available power is extracted. In PV systems, a mechanism that allows the research and tracking of the maximum power point (MPPT) is used so that the maximum power of the photovoltaic panel is permanently generated in any environmental or ambient condition [7].

The goal of the MPPT system is to generate the switching signals for the DC-DC converter similar that the maximum power can be attained from the PV panel under any ambient conditions [8]. In recent years, multitudinous MPPT schemes have been introduced that differ in cost and complexity, required sensors, convergence speed, traceability, and hardware implementation [9]. The Hill Climbing (HC) and Perturb and Observe (P&O) techniques are the most well-known and used due to their simple structure, which are presented in [10]. However, this algorithm is not effective in a steady state. Indeed, it converges around the true maximum power point and as result, a high ripple occurs in the voltage [11]. Incremental conductance (IC) is yet another technique that is useful, simple,

* Corresponding author: F Z. Boukahil, LGEB Laboratory, University of Biskra, BP 145 RP, 07000 Biskra, Algeria, E-mail: fatima.boukahil@univ-biskra.dz

¹ LGEB Laboratory, University of Biskra, BP 145 RP, 07000 Biskra, Algeria

² LMSE Laboratory, University of Biskra, BP 145 RP, 07000 Biskra, Algeria

³ University Abess Laghrour of Khenchela, BP 1252, 40004 Khenchela, Algeria

and utilizes the change in instantaneous conductance with respect to the current operating point to decide the direction of the operating point, where the PV panel must be separated to measure the open-circuit voltage or short-circuit current [12]. In spite of the easy implementation and the low cost of these methods, under rapidly changing ambient conditions their drawbacks become prominent and they fail to track actual MPP, due to their lack of properties, in terms of adaptively and robustness [13]. Sliding-Mode Control (SMC) is one of the effective nonlinear robust control approach techniques, which owns elegant features of effective disturbance rejection, fast response, and considerable robustness [14, 15].

Under partial shading conditions (PSCs), the PV characteristic curves will appear with multiple peaks (global maximum power point GMPP and local maximum power point LMPP), and using the previous MPPT technologies to track real MPP becomes a difficult task [13, 16]. For this reason, recently, other adaptive algorithms such as extremum-seeking control (ESC) and modified extremum-seeking control have been proposed [17]. Extremum Seeking Control (ESC) is of great interest in various industrial applications. For example, ESC can be utilized for maximum power point tracking (MPPT) in renewable energy systems such as wind turbines, photovoltaic micro converters, and alternator-based energy conversion systems [18].

This paper is arranged as follows: Following the introduction, Section 2 presents explicit modeling of the standalone PV system. In Section 3, the proposed first-order SMC and ESC MPPT methods are explained as techniques to track the global PV optimum point regardless the shading phenomenon that occurs during a day. To test the performances of both strategies, section 4 exhibits the obtained experimental results using a DSpace 1104 card, while section 5 concludes the work.

2. Notation

The notation used throughout the paper is stated below.

Indexes:

pv	photovoltaic
op	optimal or maximum

Constants:

q	Electron charge
k	Boltzman constant
E	Irradiance [W/m^2]
I_0	Saturation current [A]
A	Ideality factor
n_s	cellules numbers
N_s, N_p	Series and shunt panel numbers
R_s, R_p	array series, shunt resistance [Ω]
I_{cc}	Photovoltaic short circuit [A]
V_{pv}	Photovoltaic array voltage [V]
I_{pv}	Photovoltaic array current [A]
I_{ph}	Photon current [A]
I_D	Diode current [A]
V_{oc}	PV open circuit voltage [V]
T_c	Actual cell temperature [$^{\circ}K$]

Abbreviations :

<i>GPV</i>	Photovoltaic Generator
<i>ESC</i>	Extremum Seeking Control
<i>PO</i>	Perturb and Observe
<i>IC</i>	Incremental Conductance
<i>HC</i>	Hill Climbing
<i>MPPT</i>	Maximum Power Point Tracking
<i>LMPP</i>	Local Maximum Power Point
<i>GMPP</i>	Global Maximum Power Point
<i>STC</i>	Standard Test Conditions
<i>PSC</i>	Partial Shading Conditions
<i>UIC</i>	Uniform Irradiance Condition
<i>LPF</i>	Low pass Filter

3. PV system modelling

The photovoltaic system studied in this work is illustrated in figure 1. The system structure consists of two series Monocrystalin 75 Wp PV modules, connected to a resistive load via a conventional boost converter. Details of each component are described in Appendix. Prior to present the proposed control techniques, the modeling of each component is given first.

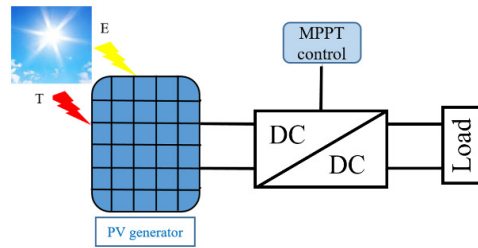


Figure 1. Schematic of the PV system.

3.1. Solar module model

Among the different modelling structures found in the literature [19], that explain the photovoltaic conversion, the famous single diode model, with four parameters (I_{ph} , I_{pv} , V_{pv} , R_s), displayed in figure 2, reproduces the experimental I-V characteristic of a mono-crystalline module with acceptable accuracy.

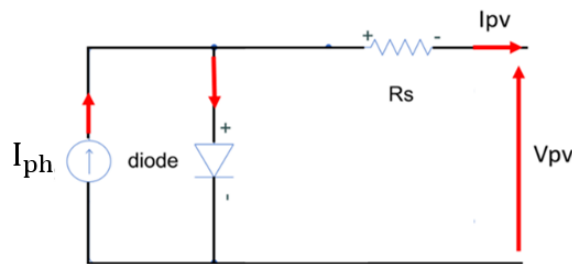


Figure 2. Single diode model of a PV cell.

The relationship between the PV voltage and current of the module is obtained via the famous non-linear implicit equation [7]:

$$I_{pv} = I_{ph} - I_0 \left[\exp \left(\frac{V_{pv} + R_s I_{pv}}{V_{th}} \right) - 1 \right] \tag{1}$$

Where the saturation current of the diode I_0 is given by equation (2), which depends on temperature T (in Kelvin).

$$I_0 = I_{0r} \left(\frac{T}{T_r} \right)^3 \exp \left(\left[\frac{qE_g}{K_b A} \right] \times \left[\left(\frac{1}{T_r} \right) - \left(\frac{1}{T} \right) \right] \right) \tag{2}$$

The photo-generated current I_{ph} depends on solar irradiance E (W/m^2) and the short-circuit current of PV cell under standard conditions I_{scr} , often given by:

$$I_{ph} = \frac{E}{E_r} \left[I_{scr} + K_i (T - T_r) \right] \tag{3}$$

3.2. Boost converter modelling

To permit a quite extraction of the maximum available PV power, a boost converter is introduced between the PV generator and the load, as shown in the figure 3. It plays in fact the role of an impedance adapter. This kind of DC-DC converters is more suitable for the loads located at the right side of the optimum PV point, where the adjustment of the duty ratio allows the input impedance to match the optimum one, as can be seen in equation (4). The boost converter is generally used in PV systems, since it permits to shift moderate PV voltage values by controlling the switching duty cycle [7].

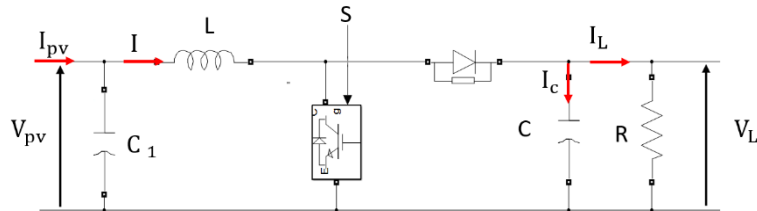


Figure 3. Boost converter circuit.

The continuous-time expressions of the boost converter can be found as follows [20]:

$$\begin{cases} \frac{dI}{dt} = -\frac{1-\alpha}{L} V_L + \frac{1}{L} V_{pv} \\ \frac{dV_L}{dt} = -\frac{1-\alpha}{C} I - \frac{1}{RC} V_L \end{cases} \tag{4}$$

The relationship between the PV and load voltage is presented in the following equation:

$$\frac{V_L}{V_{pv}} = \frac{1}{1 - \alpha} \quad (5)$$

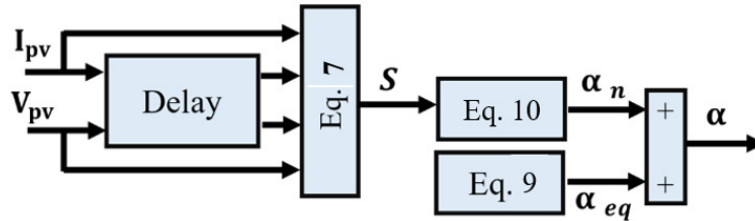
4. Control approaches

4.1. Sliding mode MPPT controller:

This control strategy, as part of the robust control system, has generally been used as a reliable tool for regulating electromechanical systems and parametric variations. In recent years, the first-order and higher-order sliding mode (super-twisting) has been successfully implemented as an MPPT algorithm [21]. In this work, only the first order sliding mode is used. The concept of the approach can be introduced by selecting the sliding surface S . Slotine [22] proposes in (6) a common equation of the surface used in electromechanically based systems. This latter lies the sliding surface, the tracking error 'e', and the relative degree 'r'.

$$S = \left(\frac{d}{dt} + \gamma \right)^{r-1} e(t) \quad (6)$$

As depicted in equation (4), the liberty degree ' α ' appears in the first equation and consequently the relative degree equals 1, which reduces in fact the sliding surface to the tracking error, defined as the incremental conductance condition to extract the maximum



power. Figure 4 shows the Sliding mode control (SMC) diagram applied for PV system.

Figure 4. Sliding mode control (SMC) diagram.

The sliding surface S is defined by:

$$S = \frac{dI_{pv}}{dV_{pv}} V_{pv} + I_{pv} \quad (7)$$

The PV system achieves the MPP when the sliding surface equals zero ($S=0$). In order to ensure this over the entire operating range, it is enough that the time derivative of the quadratic Lyapunov ($V=1/2S^2$) must be negative:

$$\dot{V} = S \times \dot{S} < 0 \quad (8)$$

The SMC is composed of two parts: α_{eq} and α_n . The first one deals with the equivalent control quantity and the second one provides the stabilization part as shown in equations 9 and 10, respectively:

$$\alpha_{eq} = 1 - \frac{V_{pv}}{V_L} \tag{9}$$

$$\alpha_n = -k.S \tag{10}$$

The duty cycle variation in the allowable range can be guaranteed if the control gain k is not selected too large. It is in fact chosen as the inverse of continuous variation of the duty cycle in the specified range can be ensured without violation if the scaling constant K is not selected too large: chosen as the inverse of the maximum equivalent load on the DC side: $k \leq |R(\max)|$, [23]:

$$R(\max) = \frac{V_{dc_min}^2}{P_{min}} \tag{11}$$

Where V_{dc_min} denotes the mean value of the PV voltage, obtained with a regular irradiance changing, while P_{min} expresses the minimum extracted power after sunshine.

4.2. Extremum Seeking MPPT Controller:

The approach can be applied to the PV system by the scheme of Figure 5. The scheme consists of the nonlinear P_{pv} , an integrator, two filters (High Pass Filter HPF and Low Pass Filter LPF) and a small sinusoidal signal. This signal is added to the PV power with the same frequency of the dither signal that is extracted through a High Pass Filter (equation 12). The gradient function is the modulation by adding a sinusoidal perturbation signal ($\sin(\omega t)$) with a relatively high frequency. Then, the low-pass filter (equation 13) eliminated unnecessary components and the resulting signal represented the estimated gradient [24]. The LPF output is applied to an integrator and added to $k * (\sin(\omega t))$ to obtain the reference PV voltage V_{pv}^* . The ESC objective is to force the operating point to be closer to the optimum for an unknown nonlinear system. This method has all the advantages of SMC such as simplicity, performance, robustness and in addition, it tracks the global MPP under different case of shading.

$$HPF = \frac{s}{s + \omega_h} \tag{12}$$

$$LPF = \frac{\omega_l}{s + \omega_l} \tag{13}$$

To ensure the convergence of the ESC controller, the cut-off frequency ω_h must be lower than the frequency ω_l , and these two frequencies are much smaller than w [24].

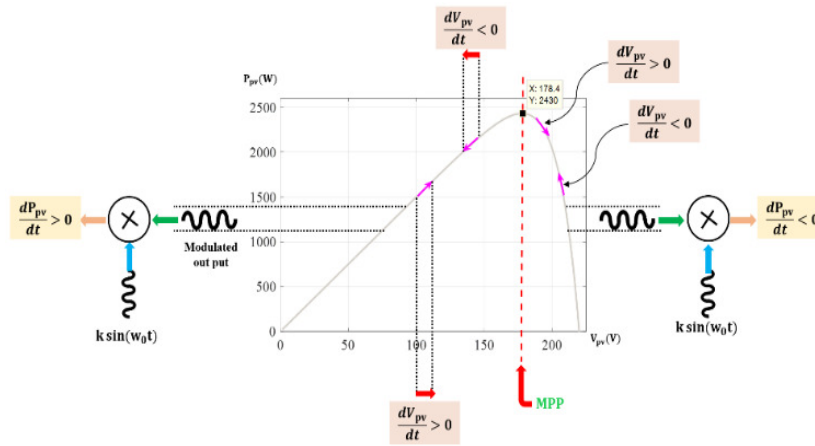


Figure 5. Scheme of the ESC based MPPT

The following figure represents the sinusoidal ESC principal applied to the PV source.

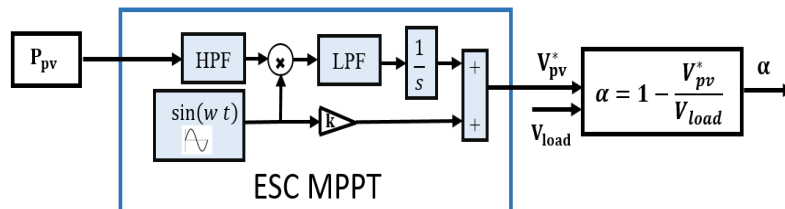


Figure 6. Extremum seeking control (ESC) diagram.

5. Experimental results

To implement and validate the above control strategies, an experimental test bench shown in figure 7, was built within the electrical engineering laboratory of Biskra (LGEB). It consists mainly of two PV modules of 170 Wp, with the parameters given in table 1; a boost converter, composed of one SKM50123, IGBT module, switched at 15 kHz, that supply a variable resistive load . A DSpace 1104 card from Texas instruments with a TMS32F240 DSP using Matlab/Simulink environment is used to implement the control algorithms proposed in this article. An interface card is used to adapt the control signal levels between the DSpace board and the power converter. Hall Effect sensors LA25NP and LV25P have been used to get respectively the different currents and voltages. To test the robustness of the proposed algorithms of maximum power point tracking (MPPT), three cases are distinguished.

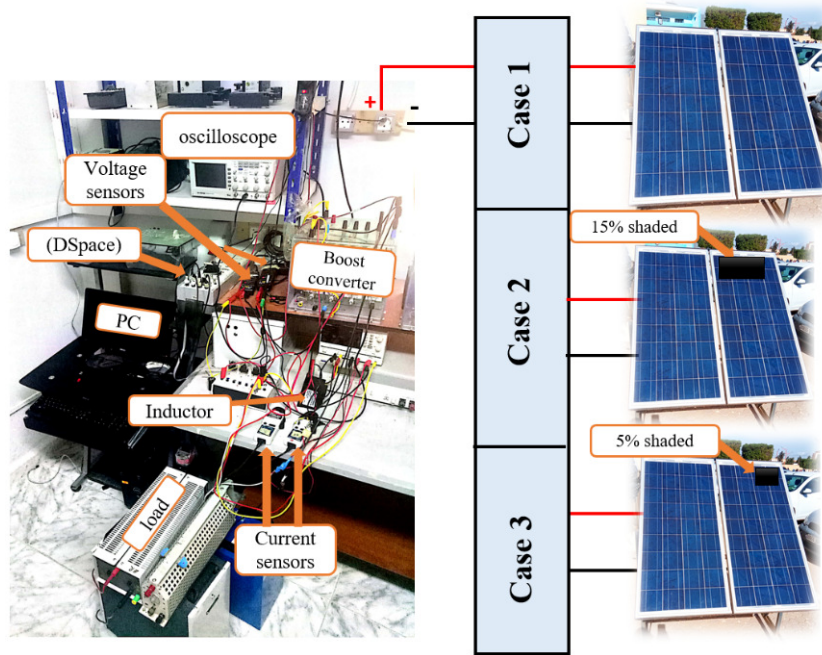


Figure 7. Test bench for experimental validation of the proposed algorithms.

The ES and SM control strategies are tested for three scenarios, in the same day (10th February 2022). The first one is the healthy case (without shading) for which the PV generator was tested under different loads and the characteristics was simulated. As can be seen in figure 8, in such situation, the so-called global MPPT point (GMPP) of 150 W is then tracked. Afterwards, the generator underwent another scenario where the GPV was made under 15 % of shading. In the last scenario, the GPV was made under a less shading ratio, of about 5%. As depicted in Figure 8, which exhibits the three cases: the bleu curve expresses the healthy case, the red one presents the 2nd case and the green one is accorded to the third case. One notices the presence of local optimum points, located at the left of the I-V curve.

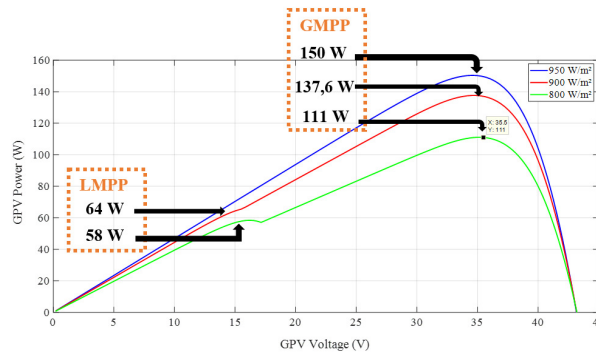
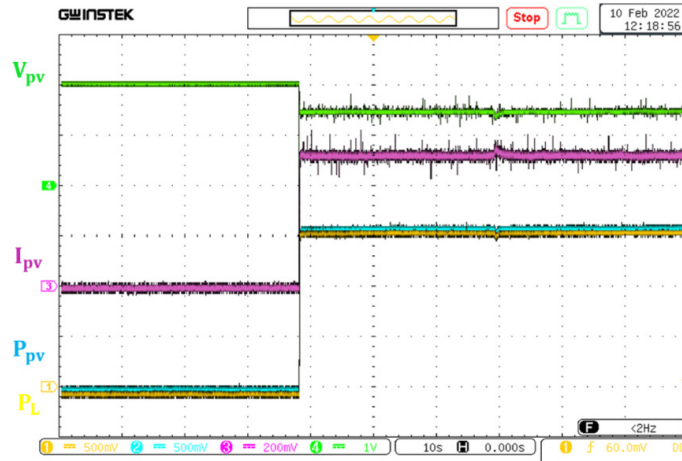


Figure 8. P-V curve of the simulation shading applied on the GPV

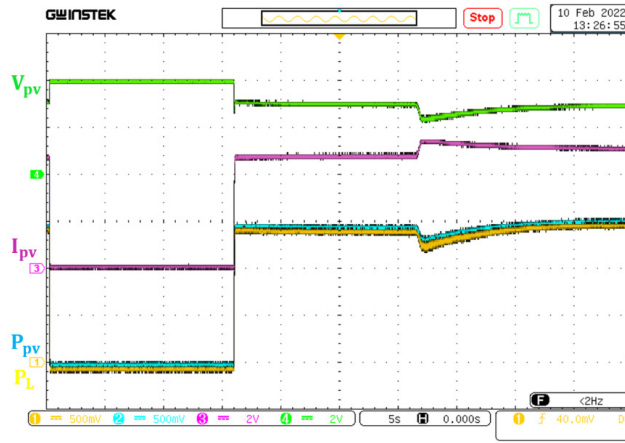
Case 1: The practical responses of the load side power and PV power, voltage, and current are shown in Figure 9. These results concern the application of the SMC and ESC algorithms under load variation. The curves are divided into three time windows: In the first time span, an initial open circuit phase is distinguished, followed by the implementation of both algorithms, and finally, a load variation is then applied. The first phase started from 0s until 40s using the SMC strategy, while just for 15 s of time span using the ESC. As remarked, in this second phase, both methods success to track the optimum point, and where the PV power is rapidly pulled to its maximum value of 150W. Accordingly, the (I_{pv}, V_{pv}) dipole converge towards their optimum values of 4A and 35V. It is noteworthy that the results of the SMC are full of chattering phenomenon, caused by the application of the ‘sign’ component of the stabilization control part whereas, smooth curves are noticed in the ESC based strategy. For the load changing, this latter is made at 70s using the SMC, and after 32s in the ESC. As can be remarked, the dynamic performance differs from one method to another. For the SMC, and thanks to the stabilization control part, the algorithm arrives to reject this load changing, in only 2s and the optimum power is then extracted again. For the ESC, the phenomenon is much longer, where the optimum point is re-tracked after 7s.

Table 1. PV module parameter

Type	Monocrystallin (Sharp) NTR5E3E/ NT175E1
Maximum power	$P_{max} = 85W$
Optimum current	$I_{op} = 4,77A$
Optimum voltage	$V_{op} = 17,9V$
Open circuit voltage	$V_{oc} = 22V$
Open circuit current	$I_{cc} = 5,2A$



(a) SMC



(b) ESC

Figure 9. Power, Voltage and Current graphs of SMC, ESC methods for case 1.

The next two cases represent the application of the two shaded ratios, where each curve is divided in three steps:

- 1st step [0, 15]s: open circuit phase
- 2nd step [15, 30]s: MPPT application
- 3rd step [30, 50]s: shading percentage application

Case 2: The performances of the two applied strategies are respectively shown in Figure 10 and Figure 11. From these figures, three remarks are extracted:

- After the initialization phase, both methods success to match the optimum point in the healthy state.
- After the application of 15% partial shading, the performance of the two applied strategies differ. As can be seen that the ESC arrives to reject the localization of the operating point at a local knee of the I-V characteristic, and converges after 0.3s to the global Maximum Power Point, and where 111 W is extracted.
- For the SMC strategy, only 58 W is tracked after 0.14s. This power concerns the local optimum point given in the green curve of Fig 8 (LMPP). At this situation and since the algorithm do not encompass a random search, while the stabilization control part success to converge to the surface equals zero, the process stops. The algorithm fails accordingly to disturb the functioning point

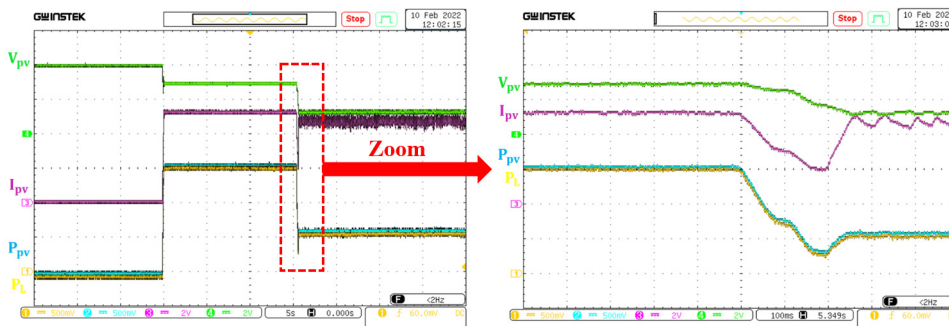


Figure 10. Power, Voltage and Current graphs of SMC method for case 2.

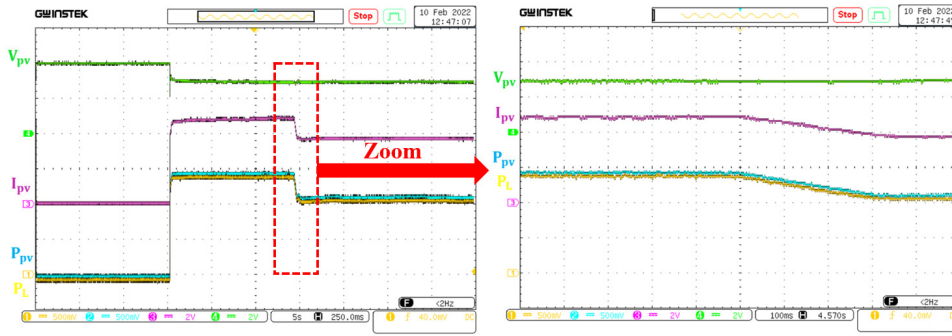


Figure 11. Power, Voltage and Current graphs of ESC method for case 2.

Case 3: In Figure 12, and Figure 13 are represented the PV and load power, PV voltage and current of the SMC and ES method, respectively for the third case. As can be seen that the ESC provides better performances, where a global MPPT power point is tracked, of about 137 W, after 2s, whereas the operating point stands at a local MPPT (LMPP), and where only 64 W was extracted after 0.36s. This point concerns in fact the red curve, plotted in Figure 8

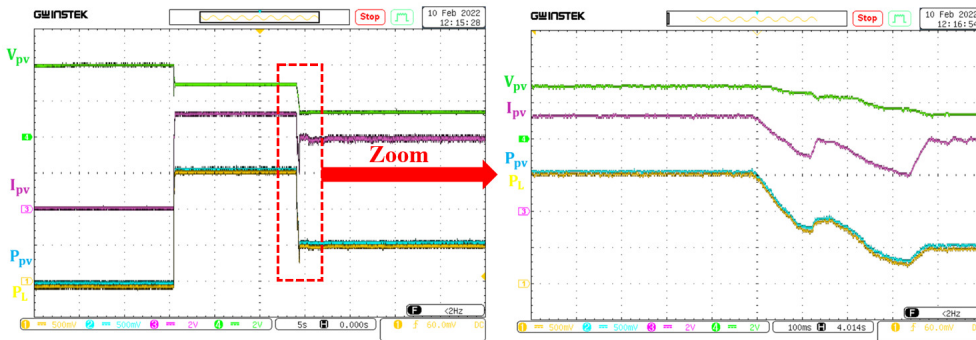


Figure 12. Power, Voltage and Current graphs of SMC method for case 3.

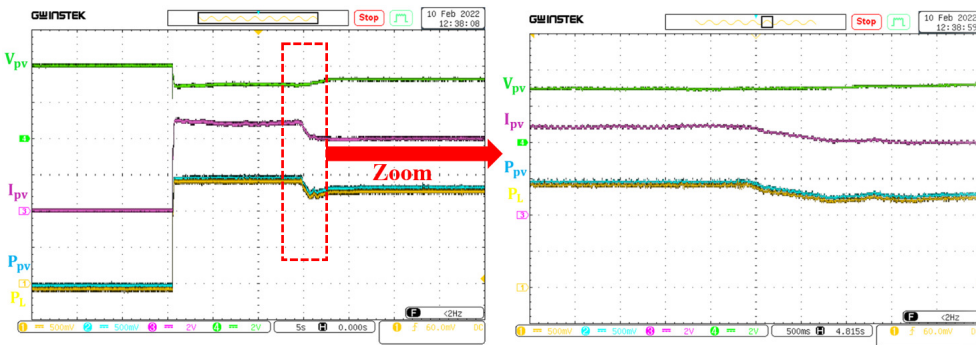


Figure 13. Power, Voltage and Current graphs of ESC method for case 3.

As a result of the implementation performance delivered by the proposed algorithms, an analysis of the tracking skills is presented in Table 2. From this table, one can obviously deduce that the SMC method presents better results than the ESC in kind of the time response to track the optimum point, while the ESC ensures the convergence to a global optimum point in case of partial shading.

Table 2. Performances comparison between SMC and ESC methods

	method	Convergence time to reach MPP (s)	MPPT
Case 1	SMC	2	Pmax
	ESC	7	Around Pmax
Case 2	SMC	0.14	LMPPT
	ESC	0.3	GMPPT
Case 3	SMC	0.36	LMPPT
	ESC	2	GMPPT

6. Conclusion

This paper investigated a real-time implementation of sliding mode and Extremum Seeking applied to attract the MPP of PV System. The application concerns the application of a partial shading with different ratios. The obtained experimental results show that the SMC-based MPPT provides a fast response under regular irradiance and load changing, but with oscillation noticed around the optimum. On the other hand, the proposed ESC strategy has proven its ability to converge to the GMPP in case of partial shading.

References

- [1] Hayat, M.B., et al., Solar energy—A look into power generation, challenges, and a solar-powered future. *International Journal of Energy Research*, 2019. 43(3): p. 1049-1067.
- [2] Shaikh, M.R.S., A review paper on electricity generation from solar energy. 2017.
- [3] Mancini, F. and B. Nastasi, Solar energy data analytics: PV deployment and land use. *Energies*, 2020. 13(2): p. 417.
- [4] Liu, C.-L., et al. A PSO-based MPPT algorithm for photovoltaic systems subject to inhomogeneous insolation. in *The 6th International Conference on Soft Computing and Intelligent Systems, and The 13th International Symposium on Advanced Intelligence Systems*. 2012. IEEE.
- [5] Huynh, D.C. and M.W. Dunnigan, Development and comparison of an improved incremental conductance algorithm for tracking the MPP of a solar PV panel. *IEEE transactions on Sustainable Energy*, 2016. 7(4): p. 1421-1429.
- [6] De Brito, M.A.G., et al., Evaluation of the main MPPT techniques for photovoltaic applications. *IEEE transactions on industrial electronics*, 2012. 60(3): p. 1156-1167.
- [7] Ali, A.I., M.A. Sayed, and E.E. Mohamed, Modified efficient perturb and observe maximum power point tracking technique for grid-tied PV system. *International Journal of Electrical Power & Energy Systems*, 2018. 99: p. 192-202.
- [8] Sampaio, P.G.V. and M.O.A. González, Photovoltaic solar energy: Conceptual framework. *Renewable and Sustainable Energy Reviews*, 2017. 74: p. 590-601.
- [9] Ayop, R. and C.W. Tan, A comprehensive review on photovoltaic emulator. *Renewable and Sustainable Energy Reviews*, 2017. 80: p. 430-452.
- [10] Fatemi, S.M., M.S. Shadlu, and A. Talebkhah. Comparison of three-point P&O and hill climbing methods for maximum power point tracking in PV Systems. *The 10th International Power Electronics, Drive Systems and Technologies Conference (PEDSTC)*. 2019. IEEE.
- [11] Youssef, A., M. El Telbany, and A. Zekry, Reconfigurable generic FPGA implementation of fuzzy logic controller for MPPT of PV systems. *Renewable and Sustainable Energy Reviews*, 2018. 82: p. 1313-1319.
- [12] Khadidja, S., M. Mountassar, and B. M'hamed. Comparative study of incremental conductance and perturb & observe MPPT methods for photovoltaic system. *The International Conference on Green Energy Conversion Systems (GECS)*. 2017. IEEE.
- [13] Refaat, A., M.H. Osman, and N.V. Korovkin, Current collector optimizer topology to extract maximum power from non-uniform aged PV array. *Energy*, 2020. 195: p. 116995.

- [14] Yang, B., et al., Perturbation observer based fractional-order sliding-mode controller for MPPT of grid-connected PV inverters: design and real-time implementation. *Control Engineering Practice*, 2018. 79: p. 105-125.
- [15] Latifi, M., et al., Improved krill herd algorithm based sliding mode MPPT controller for variable step size P&O method in PV system under simultaneous change of irradiance and temperature. *Journal of the Franklin Institute*, 2021. 358(7): p. 3491-3511.
- [16] Zafar, M.H., et al., Group teaching optimization algorithm based MPPT control of PV systems under partial shading and complex partial shading. *Electronics*, 2020. 9(11): p. 1962.
- [17] Tchouani Njomo, A.F., et al., A modified ESC algorithm for MPPT applied to a photovoltaic system under varying environmental conditions. *International Journal of Photoenergy*, 2020.
- [18] Krstic, M., A. Ghaffari, and S. Seshagiri. Extremum seeking for wind and solar energy applications. in *Proceeding of the 11th World Congress on Intelligent Control and Automation*. 2014. IEEE.
- [19] Dey, B.K., et al. Mathematical modelling and characteristic analysis of Solar PV Cell. *IEEE 7th Annual Information Technology, Electronics and Mobile Communication Conference (IEMCON)*. 2016. IEEE.
- [20] Lashab, A., et al., Discrete model-predictive-control-based maximum power point tracking for PV systems: Overview and evaluation. *IEEE Transactions on Power Electronics*, 2017. 33(8): p. 7273-7287.
- [21] Djilali, L., E.N. Sanchez, and M. Belkheiri, First and high order sliding mode control of a dfig-based wind turbine. *Electric Power Components and Systems*, 2020. 48(1-2): p. 105-116.
- [22] Slotine, J.-J.E., Sliding controller design for non-linear systems. *International Journal of control*, 1984. 40(2): p. 421-434.
- [23] Menadi, A., *Commande Par Les Techniques Intelligentes D'un Système Photovoltaïque Connecté Au Réseau*, 2016, UNIVERSITY MOHAMED KHIDER BISKRA.
- [24] Balraj, R. and A.A. Stonier, A novel PV array interconnection scheme to extract maximum power based on global shade dispersion using grey wolf optimization algorithm under partial shading conditions. *Circuit World*, 2020

© 2022. This work is published under
<https://creativecommons.org/licenses/by/4.0/legalcode>(the“License”).
Notwithstanding the ProQuest Terms and Conditions, you may use this
content in accordance with the terms of the License.